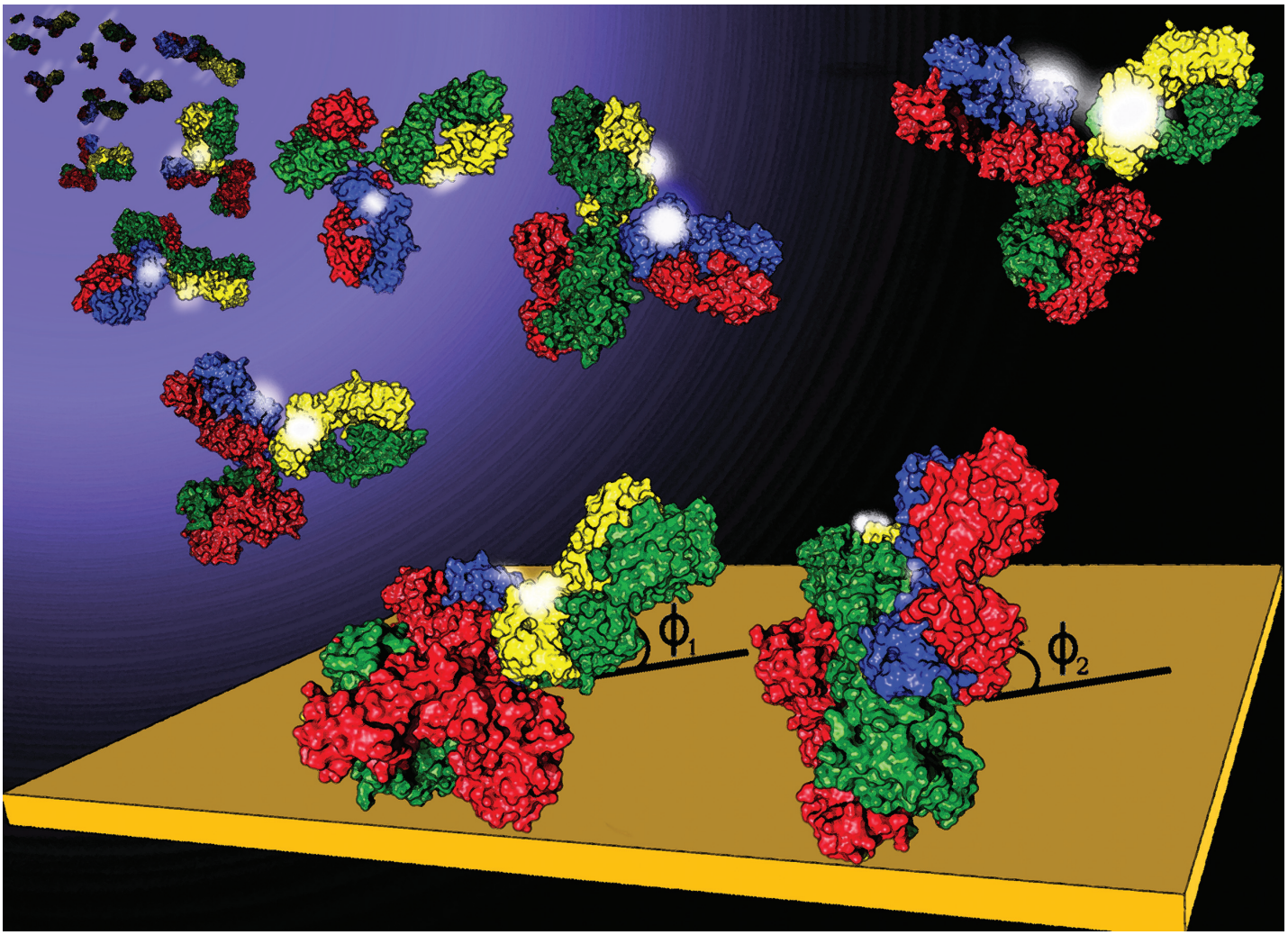

Showcasing research from Professor Raffaele Velotta's laboratory, Department of Physics "Ettore Pancini", University of Naples "Federico II", Naples, Italy.

Biosensor surface functionalization by a simple photochemical immobilization of antibodies: experimental characterization by mass spectrometry and surface enhanced Raman spectroscopy

It is demonstrated that under appropriate UV irradiation, only two disulphide bridges in IgGs are effective for covalent binding. They are located in the constant region of the IgG light chains and the UV produced thiols are reactive for several minutes, a time that suffices to convey the antibodies onto a thiol reactive surface by a suitable fluidic circuit. Eventually, the "side on" position the IgGs take up allows one of the two Fabs to sway in the solution making such a photochemical approach a valuable tool for surface functionalization.

As featured in:

See Raffaele Velotta *et al.*, *Analyst*, 2019, **144**, 6871.

ROYAL SOCIETY OF CHEMISTRY | Celebrating IYPT 2019

rsc.li/analyst

Registered charity number: 207890

Analyst

PAPER

View Article Online
View Journal | View Issue

Cite this: *Analyst*, 2019, **144**, 6871

Biosensor surface functionalization by a simple photochemical immobilization of antibodies: experimental characterization by mass spectrometry and surface enhanced Raman spectroscopy†

Bartolomeo Della Ventura,[a] Martina Banchelli,[b] Riccardo Funari,‡[c] Anna Illiano,[d] Marella De Angelis,[b] Paola Taroni,[a] Angela Amoresano,[d] Paolo Matteini[b] and Raffaele Velotta*[c]

Received 8th March 2019,
Accepted 9th October 2019

DOI: 10.1039/c9an00443b

rsc.li/analyst

Surface functionalization is a key step in biosensing since it is the basis of an effective analyte recognition. Among all the bioreceptors, antibodies (Abs) play a key role thanks to their superior specificity, although the available immobilization strategies suffer from several drawbacks. When gold is the interacting surface, the recently introduced Photochemical Immobilization Technique (PIT) has been shown to be a quick, easy-to-use and very effective method to tether Abs oriented upright by means of thiols produced *via* tryptophan mediated disulphide bridge reduction. Although the molecular mechanism of this process is quite well identified, the detailed morphology of the immobilized antibodies is still elusive due to inherent difficulties related to the microscopy imaging of Abs. The combination of Mass Spectrometry, Surface-Enhanced Raman Spectroscopy and Ellman's assay demonstrates that Abs irradiated under the conditions in which PIT is realized show only two effective disulphide bridges available for binding. They are located in the constant region of the immunoglobulin light chain so that the most likely position Ab assumes is side-on, *i.e.* with one Fab (*i.e.* the antigen binding portion of the antibody) exposed to the solution. This is not a limitation of the recognition efficiency in view of the intrinsic flexibility of the Ab structure, which makes the free Fab able to sway in the solution, a feature of great importance in many biosensing applications.

1. Introduction

Quantification of biological or biochemical processes is of utmost importance for medical, biological and biotechnological applications making biosensor development an attractive research field for its enormous potential impact in daily life.[1,2] Biosensors are analytical devices integrating a layer of biomolecules (bioreceptor) eligible for molecular recognition, and a signal transducer. Enzymes,[3,4] antibodies (Abs),[5,6] nucleic acids[7] and aptamers[8] are examples of bioreceptors widely used in biosensing although molecularly imprinted polymers (MIPs) are attracting noticeable interest for their larger stability.[9,10] MIPs are artificial receptors that mimic natural recognition biomolecules with a predetermined selectivity and specificity for a given analyte; thus they can be used as an ideal material in various applications, in particular for replacing the natural receptor molecules in biosensing.[11] Nevertheless, MIPs show several drawbacks in their quite complex synthesis (beads, membranes, *in situ* prepared monoliths) and in the subsequent surface imprinting[12] so that "natural" bioreceptors are still a standard in biosensor design. In this respect, in spite of some possible limitations, antibodies are prime candidates to be used for biorecognition as they are exquisitely designed and engineered to this aim.[13]

The immunoglobulin G (IgG) is a typical Ab with a molecular weight of approximately 150 kDa, tens of nanometers in size, and a characteristic Y-like shape (Fig. 1). The Fragment

[a]*Dipartimento di Fisica, Politecnico di Milano, Piazza Leonardo da Vinci 32, 20133 – Milano, Italy*
[b]*IFAC-CNR, Istituto di Fisica Applicata 'Nello Carrara', via Madonna del Piano 10, 50019 Sesto Fiorentino, Italy*
[c]*Dipartimento di Fisica "Ettore Pancini", Via Cintia, 26, 80126 – Napoli, Italy. E-mail: rvelotta@unina.it*
[d]*Dipartimento di Scienze Chimiche, Via Cintia, 26, 80126 – Napoli, Italy*
†Electronic supplementary information (ESI) available. See DOI: 10.1039/c9an00443b
‡Present address: Okinawa Institute of Science and Technology, Graduate University, 1919-1 Tancha, Onna-son, Okinawa, 904-0495 Japan.

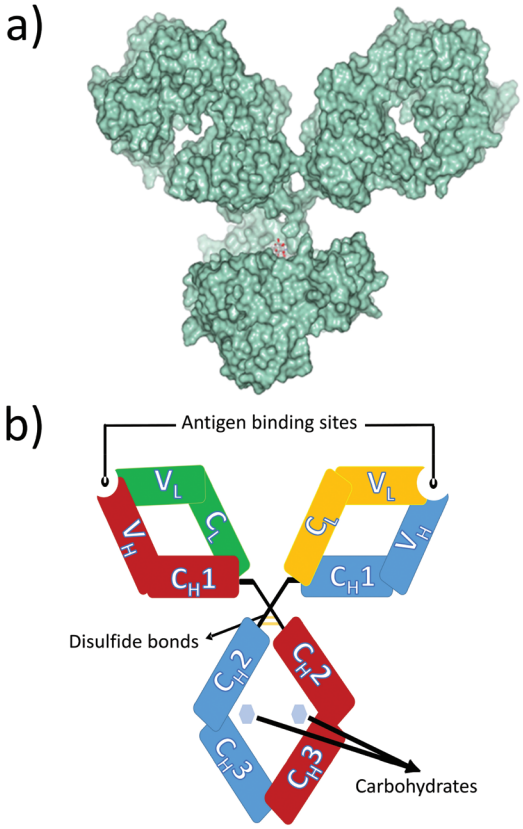

Fig. 1 (a) Spherical representation of 1IGY from the protein databank based on its X-ray crystallographic structure. (b) Block scheme of an IgG. The heavy chain is formed by one variable domain (V_H) and three constant domains (C_H), whereas the light chain includes the light (V_L) and heavy (V_H) domains.

antigen binding (Fab) domain contains the complementarity-determining regions which constitute the antigen-binding sites of the Ab providing its characteristic high antigen specificity.[14] The possible orientations an Ab can assume on a surface can be grouped in four categories (Fig. 2):[5,15] tail-on and side-on, in which at least one Fab is free to move and exposed to antigens, as well as head-on and flat-on corresponding to both Fabs hidden and, hence, unavailable for antigen recognition. Since the Ab orientation determines the overall performance of the device to a large extent,[16] the procedure used for the surface functionalization proves to be a crucial step in designing an immunosensor.

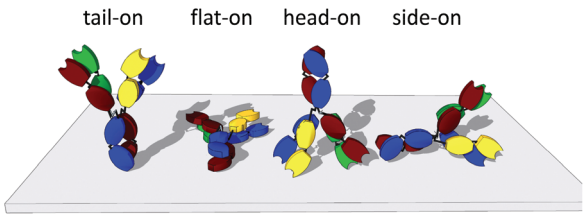

Fig. 2 Possible positions Ab can take up on the surface.

Relying on non-covalent interactions (*e.g.* van der Waals forces or electrostatic interactions), Abs can be easily tethered to a surface, but the resulting bonds suffer from two main drawbacks, *i.e.* the poor bond strength and, even more important, the random orientation of Abs. The latter issue can be overcome by resorting to intermediate proteins (*e.g.* protein A and protein G) that bind the Fc region of the antibody so that the tail-on orientation is favored. However, this non-covalent approach becomes critical in protein-antibody disassembling during the regeneration of the biosensor,[6] an issue made more acute by the length of the functionalization procedure. Moreover, a possible involvement of the protein affinity domain in the interaction with the surface might even lead to sub-optimal immobilization.[17]

Stronger bonds can be achieved by modifying the biosensor surface with reactive groups such as hydroxy, thiol, carboxy or amino groups for the subsequent Ab covalent immobilization.[18] However, the chemistry involved in these procedures is usually complex and time-consuming so that the whole production process turns out to be demanding.[19] Moreover, the covalent conjugation of Abs onto solid surfaces by using chemical linkers does not guarantee high antigen binding efficiency in view of the possible modification of the antigen binding sites as well as the lack of control on protein orientation.[20,21] A higher degree of orientation can be achieved by making photoactivatable the Fc region of the Ab, so that the latter can be site-selectively immobilized, but the whole strategy is quite complex and requires a previously prepared surface.[22,23]

Alternative surface functionalization strategies rely on the immobilization of Ab fragments rather than the whole antibody; in particular, half antibodies as capture probes were immobilized onto gold[24,25] and zinc surfaces.[26] Recently, half Abs were even tethered to a vinyl functionalized glass surface by means of a UV light induced thiol–ene coupling reaction.[27] A direct photochemical reaction (no auxiliary reagents used) is also at the basis of the Light Assisted Molecular Immobilization (LAMI),[28] which has led to the immobilization of antibody Fab fragments onto a chemically treated quartz slide.[29] Such an approach proved to be effective in producing microarrays though it requires a laser source that warrants both high UV light intensity and spatial resolution.[30] Generally, however, the production of IgG fragments requires a proper chemical reduction of the whole Ab,[31] which may affect its binding capacity.[32]

LAMI was also recently used to immobilize whole Abs onto a chemically treated surface, although by using the third harmonics of a femtosecond Ti:Sapphire laser.[23] Thus, in an effort towards the achievement of a simple and effective surface functionalization and relying on the same molecular mechanism underlying LAMI, we setup a procedure that includes two steps: (1) activation of *whole* IgGs in solution by a high intensity UV lamp and (2) subsequent transfer of the solution to the biosensor surface for Ab surface binding. Such a procedure was termed Photochemical Immobilization Technique (PIT) and differs from LAMI in that in the former

the UV activation of antibodies takes place away from the surface to be functionalized rather than in its proximity. As for LAMI, PIT is based on the selective photoreduction of the disulfide bridge in some of the cysteine–cysteine/tryptophan (Cys–Cys/Trp) triads,[33] which are a typical structural feature of the IgG.[34] The UV-excitation of the Trp residue leads to the generation of solvated electrons, which are captured by the nearby disulfide bridge resulting in its destabilization and subsequent breakage of the cysteine–cysteine bond. The as-produced free thiol groups interact with the proximal metal surface giving rise to an oriented covalent IgG immobilization ultimately enhancing the antigen detection efficiency of the immunosensor as already demonstrated with quartz-crystal microbalances (QCMs) in the detection of small analytes[35,36] as well as of heavy antigens.[37,38] Recently, PIT was successfully applied also to the detection of bacteria[39] and was extended even to plasmonic sensors,[40,41] overall demonstrating that the controlled UV irradiation used in PIT does not affect the intrinsic selectivity of the antibodies,[35–41] The above surface functionalization technique is simple to apply, reproducible and cost effective leading to a final 10/20-fold enhancement of the antigen-binding detection compared to randomly immobilized Abs.[35,36] Despite being routinely used to functionalize metal surfaces (gold) with high efficiency, only partial evidence of the whole mechanism underlying PIT has been reported so far,[42] whereas a clear proof of which specific amino acid triad is directly responsible for the protein immobilization upon UV light activation is still missing.

In this manuscript, we capitalize on matrix-assisted laser desorption/ionization-time of flight mass spectrometry (MALDI-TOF-MS) and Surface-Enhanced Raman Spectroscopy (SERS) analysis techniques as well as on a biochemical tool (specifically Ellman's assay) to provide detailed characterization of the PIT process aimed at identifying the functional groups responsible for the covalent binding of Abs to a metal surface. As a case study, we choose the monoclonal antibody anti-phenobarbital from host musculus since its sequence is well-known (Fig. S1†) and its crystallographic structure is available in the protein database.[43] We show that appropriate UV irradiation conditions lead to the formation of mostly four free SH groups, two of them available for Ab immobilization, ultimately offering a molecular description of the PIT mechanism. Specifically, we demonstrate that by irradiating Abs in solution for only 30 s with UV light from an amalgam type lamp ($\approx$0.5 W cm^{-2} on the sample), we are able to produce "activated Abs" showing approximately 8 reduced thiols ($\approx$4 disulphide open bridges per Ab). Once formed, these thiol residues stay reduced (active) for approximately 300 s, a time long enough to deposit Abs onto a metal (gold or silver) surface on which they bind upright. The position of the free cysteines in the polypeptide chain as generated by UV activation is determined by mass spectrometry, which also confirms that only 8 thiols per Ab are reduced by UV and 4 of them (*i.e.* 2 disulphide bridges) are not exposed to the solvent lowering to two the number of bridges available for PIT. Moreover, we observe that the SERS signal generated by UV-treated Abs appears much stronger than that coming from untreated Abs, thus demonstrating that Abs have higher proximity and extensive contact to the surface when UV activated. Finally, the knowledge of the IgG sites involved in the surface functionalization allowed us to identify the possible orientations the Abs can assume on the surface.

2. Experimental section

2.1. UV irradiation of immunoglobulins

PIT was performed by irradiating aqueous solutions of IgGs (anti phenobarbital monoclonal Ab from host musculus from antibodies-online.com, Germany) in the range of 25–70 μg mL^{-1} contained in a quartz cuvette for a variable time (0–1800 s). The UV light was produced by a HERAEUS amalgam type NNI 40/20 lamp emitting at 254 nm with a power of 40 W. The intensity of the lamp used in this experiment was about 0.7 W cm^{-2} very close to the surface. By considering that the quartz cuvette was at a distance of 1 cm from the outer edge of the lamp, the actual irradiation intensity used for the antibody activation was approximately 0.5 W cm^{-2}. Such an intensity is low enough to avoid any significant photolysis of the S–S bond that poorly absorbs at 254 nm.[44]

2.2. Reagents and procedure for Ellman's assay

5,5-Dithio-bis-2-nitrobenzoate (DTNB, purity 99%) was purchased from Sigma–Aldrich and the "phosphate buffer/6 mM DTNB" mentioned throughout the paper contained 0.1 M phosphate buffer, pH 7.4, and 6 mM of DTNB.

A quartz cuvette containing a solution of IgG (25 μg mL^{-1}) was irradiated by the UV lamp described in the previous section for times in the range of 0–1800 s. To find the optimal irradiation time, the DTNB reagent (2 mM) with ratio 1 : 2 v/v was added into the cuvette immediately after the irradiation. The optimal time for PIT turned out to be 30 s, which was the irradiation time used for studying the dynamics of the UV produced free thiols. This was realized by adding Ellman's reagent with controlled delays ("waiting time") after the 30 s irradiation. In all Ellman's assays carried out in this work, the absorbance of the anion (TNB^{2-}) at 412 nm was measured after a reaction time of 15 minutes.

2.3. MALDI-TOF mass spectrometry

All reagents were purchased from Sigma Aldrich, Milan, Italy. Different IgG solutions (25 μg mL^{-1}, 50 μg mL^{-1} and 70 μg mL^{-1}) were exposed to UV irradiation (λ = 254 nm) for 30 s, 60 s and, 90 s. Irradiated IgGs were treated with 50 mM iodoacetamide in molar excess (1 : 5) with the number of cysteine residues to block all the disulfide bonds reduced by irradiation. The reaction was carried out at room temperature for 30 min in the dark. Afterwards, the antibodies were precipitated by sequential methanol, chloroform, and water treatment and the protein pellet was recovered and dried under vacuum.

The denaturation of the IgG was performed by using 10 mM dithiothreitol (1 : 10 molar excess compared to the

number of moles of cysteine residues present in the protein) in denaturing buffer (6 M Guanidine, Trizma 300 mM, EDTA 10 mM, pH 8). The reaction was performed for 2 h at 37 °C.

Subsequently, proteins were precipitated with methanol, chloroform and water and the recovered protein pellet was subjected to tryptic digestion using an enzyme amount in 1 : 50 ratio to the amount of proteins. The peptide mixture was sub digested with chymotrypsin in a 1 : 20 ratio to the amount of processed proteins. Enzymatic digestions were carried out for 18 h at 37 °C. The peptide mixture was eventually analyzed by MALDI TOF. The experiments were performed on a 4800 MALDI-TOF-TOF ABSciex equipped with a nitrogen laser (337 nm). Calibration was preliminarily performed by using an AB SCIEX calibration mixture (Monoisotopic (M + nH)n+: 904.46 Da des-Arg-Bradykinin, 1296.68 Da Angiotensin I, 1570.67 Da Glu-Fibrinopeptide B, 2093.08 Da ACTH (clip 1–17), 2465.19 Da ACTH (clip 18–39), 3657.92 Da ACTH (clip 7–38). 0.5 μL of the sample (1/1, v/v) was mixed with a 10 mg mL^{-1} solution of α-cyano-4-hydroxycinnamic acid in 70 : 30 acetonitrile:50 mM citric acid in water solution. Spectra were acquired using a mass (m/z) range of 300–3000 Da for peptide identification.

2.4. Fabrication of AgNC-decorated QCM substrates for SERS measurements

Silver nanoparticles with a cubic shape and a size of 50 nm (AgNCs, see the ESI† for their synthesis and characterization) were deposited onto a gold-coated QCM chip by slightly modifying a previous protocol.[45,46] Briefly, n-hexane (0.4 mL) was placed in a PTFE cell (5 cm^2 area) and 0.08 mL of an aqueous nanocube suspension was added afterwards. 0.16 mL of EtOH was then dropped at the top of the hexane phase, leading to the assembly of AgNCs at the water–hexane interface. Upon complete solvent evaporation the floating AgNC assembly firmly adhered to a QCM crystal lying on the bottom of the PTFE cell. The as-formed AgNC-decorated QCM substrates were finally washed twice with water and ethanol and, after overnight drying, were subjected to a 10 min plasma treatment (ZeptoDiener Plasma Surface Technology operating at 40 kHz and 1 mbar air) before use.

2.5. Immobilisation of IgGs on the AgNC-decorated QCM substrates and QCM protocol

The fluidic circuit consisted of a cell containing the oscillator, tygon tubes, a reservoir for the solution (quartz cuvette) and a peristaltic pump.[38] The cuvette containing 0.5 mL of antibodies dissolved in milliQ water (25 μg mL^{-1}) was irradiated by UV light for 30 s (see section 2.1), which is the optimal irradiation time for PIT (see section 3.1). Immediately after the irradiation, the cuvette was placed in the fluidic circuit that conveyed the irradiated Ab solution on the AgNC-decorated QCM substrate at a flow rate of 10 μL s^{-1}.

The relationship between the frequency variation of the microbalance and the mass deposition Δm is given by the Sauerbrey equation[47] from which we have $\Delta f = -K(\Delta m)$, K being a constant depending on several experimental parameters (resonance frequency, crystal active area, quartz density and shear modulus for the AT-cut crystal). The experimental protocol for IgG immobilization included the following steps: (1) mounting of the AgNC-decorated substrate into the fluidic circuit followed by cleaning with milliQ water and basal frequency stabilization, (2) injection of the antibody solution (with and without UV irradiation) and (3) final washing step with milliQ water to eliminate the weakly bonded material. Both the injection and washing steps lasted 15 minutes. Three replicates of three substrates were prepared as described: one without antibodies contained in the buffer solution of the fluidic circuit, which was used as reference, and the other two exposed to untreated and UV-activated antibodies. The sensorgram recorded when UV treated Abs were injected into the cell is shown in Fig. S2.†

2.6. SERS

SERS measurements were carried out under a microRaman Horiba Xplora system coupled to a 532 nm diode laser. Single acquisitions of 10 s with a laser power at the sample of ≈2 mW and a diffraction grating of 1200 l mm^{-1} were performed. The backscattered signal was acquired by focusing the laser beam on the nanoparticle layer by means of a 10× microscope objective (0.25 NA), generating a ≈7 μm size beam waist that provides an average response in turn minimizing possible local signal variability. The final spectra represent the average of 50 random measurement points from 3 replicates. The Raman spectrum of a drop-cast (5 μL) aqueous solution of antibody on a gold mirror support (Thorlabs, Inc., Newton, NY) was used as reference for mode assignment. Spectra were baseline subtracted when needed.

3. Results and discussion

3.1. Ellman's assay

The breaking of disulphide bridges occurring after the UV irradiation was assessed by Ellman's assay,[48] in which the reaction of a thiol residue with DTNB reagent gives rise to mixed disulfide adducts and 2-nitro-5-thiobenzoic acid (TNB^{2-}) as products. Thiol concentration was quantified by measuring the absorbance at 412 nm (relative to the anion TNB^{2-}) after the calibration of the assay (see Fig. S3† for details on the calibration). Fig. 3 reports the absorbance at 412 nm of a solution of Abs at 25 μg mL^{-1} and the corresponding free thiols produced by UV illumination as a function of the irradiation time. The absorbance reaches a maximum after 30 s irradiation, corresponding to approximately 8 thiol residues (4 broken disulfide bridges) per Ab.

The occurrence of an optimum irradiation time (Fig. 3, black points) is explained by considering the balance between the increase of the number of free thiols induced by prolonged UV irradiation, and the degradation of the Abs, which also increases at long exposure time as a result of the absorption of the high dose of UV light. The stability of the UV-reduced disulphide bridges was also verified by adding Ellman's reagent

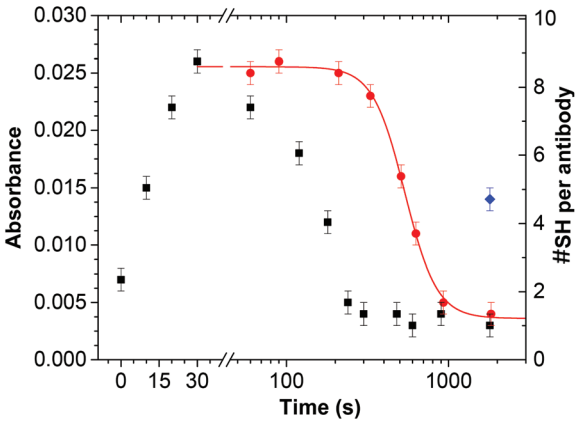

Fig. 3 (Ellman's assay). TNB^{2-} absorbance and number of free thiols per Ab as a function of irradiation time. The Ab concentration was 25 μg mL^{-1}. The black square points refer to the number of thiols yielded immediately after irradiation and show an optimum irradiation time of 30 s. A possible decrease in the number of free thiols produced after illuminating the sample for 30 s was investigated. Specifically, by adding the Ellman reagent to the latter sample after different "waiting time", we verified that the number of thiol residues remains unaltered up to 300 s (red circle points). After a waiting time of 1800 s the solution was subjected to a further 30 s irradiation, giving rise to a recovery in the number of free thiols of approximately 50% (blue diamond point).

at different times ("waiting times"). The results are shown in Fig. 3 (red points), which highlights the fact that the disulphide bridges remain open for 300 s, a time long enough to tether activated Abs to the metal surface. The degree of reversibility of the process induced by the PIT was finally tested by further irradiation of the Ab solution after a waiting time of 1800 s, a time long enough for the absorbance to return to the value measured with the initial solution (Fig. 3). In this case, a recovery of approximately 50% in the number of free thiols demonstrates that UV irradiation carried out under the conditions required for PIT induces only partial degradation processes.

3.2 MALDI-TOF-MS

Among all analytical methods used to characterize monoclonal antibodies, mass spectrometry plays an increasingly important role for both global and fine structural characterization of the structures.[49–52] Here, mass spectrometry was used to investigate which cysteine residues, pertaining to a particular disulphide bridge of the polypeptide chain of Ab, are reduced by UV irradiation.

MALDI mass mapping analysis was performed on the sub-digested standard protein UV irradiated in a time course analysis as reported in section 2.3. The molecular targets of the mass spectral investigation relied on the identification of Cys-containing peptides that were alkylated by iodoacetamide after UV irradiation. Thus, peptide mixtures were analyzed by MALDI TOF mass spectrometry and peptide identification was performed by comparing experimental *m*/*z* values detected in the mass spectra with theoretical ones. As an example, Fig. S4† reports the MALDI spectrum of 25 μg mL^{-1} of IgG digested with trypsin and chymotrypsin and exposed to UV radiation (λ = 254 nm) for 30 s (panels A and B), and the corresponding modified peptide attribution (panel C). The overall data obtained by MS investigation are reported in Table 1, which contains a comparison between the cysteine yield detected in irradiated and non-irradiated Abs. By considering a yield threshold of 5%, we found that the cysteines reduced by UV irradiation are exclusively placed in the positions 26, 86, 106, 357, 302 and 102. Cysteines found in positions 102 and 106 are also present in the control sample[53] and as such they can be discarded as the possible candidates for covalent Ab anchoring. From the analysis of the 3D structure of our Ab, it turns out that the four remaining cysteines (26–86 and 302–357) interact with each other to form the disulfide bridges, which realizes the Cys–Cys–Trp triad. These disulfide bridges are localized in the light chain constant region (26–86) and in the heavy chain constant region (302–357), respectively. Since the antibodies are composed of two identical heavy and light chains, mass spectrometry shows that UV irradiation (under the conditions required by PIT) leads to the reduction of only four disulfide bridges. Thus, the mass spectral findings are in excellent agreement with the result obtained by the Ellman assay. While cysteines 302–357 are not exposed to the solvent,[54,55] and as such it is unlikely they contribute to binding of the Ab to a surface, cysteines 26–86 are located on the external surface of the antibody and, hence, they represent the most plausible candidate in the process underlying PIT.

Table 1 Cysteines with high yield (≥5%) identified by mass spectrometry after UV irradiation carried out under the same conditions under which PIT is realized (amalgam lamp emitting at 254 nm with an intensity on the sample of ≈1 W cm^{-2} for 30 s). C102 and C106 are detected also in the control and their presence may well account for the non-zero intercept in Fig. 3. In contrast, the occurrence of C26–C86 and C302–C357 is a result of the UV irradiation

Chain	Peptide sequence	*m*/*z*	Position modified Cys	Yield after UV irradiation	Yield in untreated Ab (control)	Domain
IGKC	TSGGASVVC*F	984.46	C26 intrachain	25%	<5%	C_L
	HNSYTC*EATHK	1347.52	C86 intrachain	15%	<5%	C_L
	SFNRNEC*	926.30	C106 interchain	15%	15%	Hinge region
IGH1M	SVC*YSAAVTL	1070.51	C357 intrachain	15%	<5%	C_H3
	TC*SVLHEGL	1037.42	C302 intrachain	10%	<5%	C_H3
	DC*GCKPCICT VPEVSSVFIFPPKPK	1405.59	C102 interchain	15%	15%	Hinge region

The MALDITOF analysis was carried out at different protein concentrations (25 μg mL^{-1}, 50 μg mL^{-1} and 70 μg mL^{-1}) and different irradiation times (30 s, 60 s and 90 s). We noted the occurrence of a very low sequence coverage (only 25%) when the irradiation time was 90 s independent of the Ab concentration. On the other hand, a high sequence coverage of 75% was found when the irradiation time was set at 30 s or 60 s, but only at an Ab concentration of 25 μg mL^{-1} and 50 μg mL^{-1} since at 70 μg mL^{-1} low sequence coverage (25%) was again observed. We ascribe such a behavior to the degradation of the Abs induced by UV irradiation as analogously interpreted from the results of Ellman's assay Additionally, the observed trend at high concentration values emerging from MS analysis can be ascribed to the formation of Ab dimers or higher order aggregates as a result of the formation of highly reactive SH radicals, which are favored under UV irradiation conditions. The formation rate of the aggregates should be linearly dependent on the initial Ab concentration, but it is expected to be dependent more than linearly on the irradiation time, which also enters into the activation process. In conclusion, both Ellman's assay and the MS analysis suggest that the optimal irradiation time for PIT is approximately 30 s and the initial Ab concentration should never exceed 50 μg mL^{-1}.

3.3. SERS (surface enhanced Raman scattering)

In an attempt to gain more insights into the interactions established by Ab molecules at the interface upon UV irradiation, we decided to take advantage of the unique characteristics of SERS as an ultrasensitive vibrational spectroscopy providing a chemostructural description of the surface chemistry of a molecule placed in contact with plasmonic nanostructures. In this framework we selected a SERS substrate produced by the assembly of silver nanocubes (AgNCs), conveniently covering a QCM gold–coated quartz support with the aim of monitoring the formation of an Ab layer. Overall, we may note that AgNCs represent a convenient choice for studying bio-nano interactions due to the availability of solid synthesis protocols ensuring well-defined geometrical and optical properties[56] (Fig. S5†). In particular they show quasi single-crystal features with dominating low-energy (100) facets,[57] which largely simplify the surface chemistry guiding the protein immobilization.[58,59] Nonetheless, the application of plasmonic nanoparticles with non-spherical geometry is attracting growing interest in biosensing[60] and in other biodetection schemes[46,61] due to their amplifying antenna-like behavior. Thus in our SERS setup AgNCs act as effective nanoantennas to enhance the Raman signal of chemically or physically adsorbed IgG in such a way to allow the collection of its vibrational spectrum in spite of a low local protein density.

Initially, QCM measurements were used to inspect and, in turn, optimize the antibody immobilization by tracking mass differences when Abs are tethered on the nanoparticle surface. IgG immobilization was performed by using a microfluidic system designed to have a controlled flux of untreated or UV-treated IgG solutions onto the plasmonic surface (see the Experimental section for details). Subsequently, the samples were analysed by microRaman spectroscopy and their SERS signal (Fig. 4) was compared to the Raman profile of a dried deposit of the antibody (Fig. S6†). A nice matching between SERS and Raman spectra lets us identify the main vibrational modes of IgG as detailed in Table S1.† We observed a high point-to-point reproducibility with intensity values depending on the amount of anchored antibody. Therefore, SERS spectra were normalized considering the frequency shift obtained with the QCM measurements. A 1.5-fold increase of the band centered at 240 cm^{-1}, including modes associated with the Ag–S stretching, immediately emerges from comparing the UV-treated sample with the untreated sample (see spectra in Fig. S7a and quantitative estimation in Table S2†). We can infer that upon UV activation, light-induced breaking of disulfide bridges in the protein becomes responsible for an increased bonding of free thiol groups with the metal surface.[62] A comparable increase in the 653 cm^{-1} mode (Fig. S7b and Table S2†) supports a larger amount of C–S bonds proximal to the Ag surface, which is in line with a superior formation of Ag–S bonds once Cys residues are activated by UV radiation,[63] as observed above. Thus, these initial considerations endorse and extend previous findings from Ellman's assay and MS, being direct evidence of the potential of Ab molecules activated *via* PIT to establish covalent bonds with a metal surface. Aromatic amino acids typically display prominent signals in the Raman spectra of proteins that are extremely susceptible to plasmonic enhancement. Accordingly, Phe (F), Tyr (Y) and Trp (W) spectral signals appear up to three-fold larger in the spectrum of the UV-treated sample (Fig. S7c and d, Table S2†). Specifically, an increase in the bands characteristic of Phe, namely 1003, 1031, 1205, 1603 cm^{-1}, is well justified by a closer proximity of these residues to the plasmonic surface. In a similar fashion, Trp modes at 756, 877, 1330 and 1555 cm^{-1} and Tyr modes at 830, 850 and 1612 cm^{-1} appear more intense. Interestingly, the relative intensity of the 830 and 850 cm^{-1} doublet of Tyr appears different when

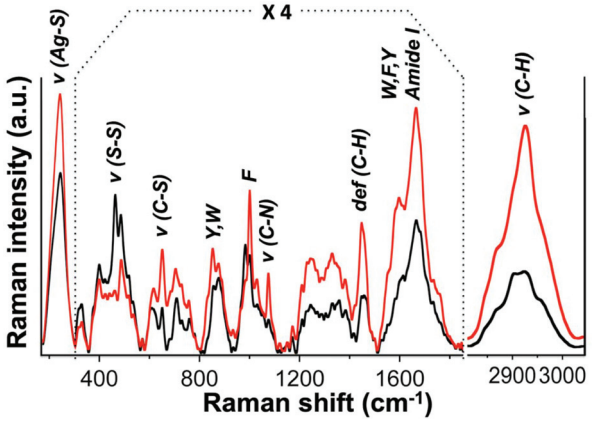

Fig. 4 Recap of representative SERS spectral regions of UV-activated (red) and non-activated (black) samples. Signals within the 400–1800 cm^{-1} region were 4× multiplied for clarity. (λ_{EX} = 532 nm; integration time = 10 s; laser power at the sample ≈2 mW).

moving from the non-irradiated to the irradiated sample. The relative intensities of the two bands are a common marker used for tertiary structure prediction because it depends on the presence of a hydrogen-bonded phenyl ring of the lateral chain.[63] Thus, a higher I_{850}/I_{830} band ratio as observed in the UV-treated sample may indicate a higher exposure of Tyr residues to the aqueous environment as a consequence of the formation of Cys/metal bonds.

The evidence of more intimate surface interactions established by UV-immobilized Abs arises from the analysis of those spectral regions characteristic of protein conformation and secondary structure. It is noteworthy that important spectral changes occur in the conformationally sensitive region of the protein skeletal modes involving C–C and C–N stretching vibrations (900–1100 cm^{-1}). Despite a significant decrease in the intensity of the band between 980 and 990 cm^{-1} (assigned to the Amide III antiparallel β-sheet mode), in the UV-treated sample a marked increase is displayed in the band centred at 1076 cm^{-1} (Fig. S7e and Table S2†), ascribed to the C–N bonds of the backbone chain. This is rightfully consistent with a very close vicinity of the IgG polypeptidic chain to the AgNC-decorated QCM substrate, to a large extent with respect to the untreated protein. Accordingly, the Amide I spectral region (around 1660 cm^{-1}), accounting for the secondary structures of the protein (Table S3†), also shows much higher intensities in the UV treated sample.

The spectral region between 2800 and 3000 cm^{-1} is characteristic of the C–H stretching of the CH_2 and CH_3 groups. These groups are placed along the whole polypeptide chain and their signals in the UV treated sample (Table S2†) appear higher than that in the untreated one (as also confirmed by the increased intensity of CH, CH_2 deformations at 1420–1480 cm^{-1}, Fig. S7f and g†). We can deduce that in the case of the UV-treated antibody a larger number of aliphatic or methylated amino acids are also forced to approach the metal surface.

The overall body of results provided by SERS brings to the conclusion that the illumination parameters used to conduct PIT on Ab molecules were adequate to promote their effective thiol-mediated surface attachment and in a larger extent that in the case of untreated Ab. Furthermore, the amplification of a large set of vibrational modes in UV-treated samples suggests that Ab anchoring could also involve an extensive contact with the surface.

3.4. Modeling the IgG morphology resulting from PIT

Two independent characterization studies (Ellman's assay and MS) demonstrated that merely 4 disulfide bridges (C26–C86 and C302–C357), among the twelve potentially involved in the process, are reduced by UV irradiation carried out under the conditions required for PIT. The photochemical reduction was revealed to occur for one of the cystines located in the constant region of the light chain (C26–C86) and for one located in the constant region of the heavy chain (C302–C357) with a yield higher for the former. To shed further light on the mechanism underlying such a selective process, we analysed the IgG structure by Protein Imager 2.0.[64] From careful scrutiny, we found that most of the twelve triads are very close to phenylalanine and tyrosine, the other aromatic amino acids other than tryptophan that can absorb UV light (Fig. 5a). Instead, only two triads, *i.e.* those containing the C26–C86 pair in both Fab domains, are far from tyrosine and phenylalanine (Fig. 5b). The remaining cysteines are fully surrounded by Phe and Tyr, whereas C302–C357 are surrounded by only Phe and, hence, able to undergo photo-chemical reduction although at a lower rate as it turns out from MS measurements. On the other hand, the bridge C302–C357 is quite unexposed to the solvent,[54,55] and as such it is unable to bind the surface. Thus,

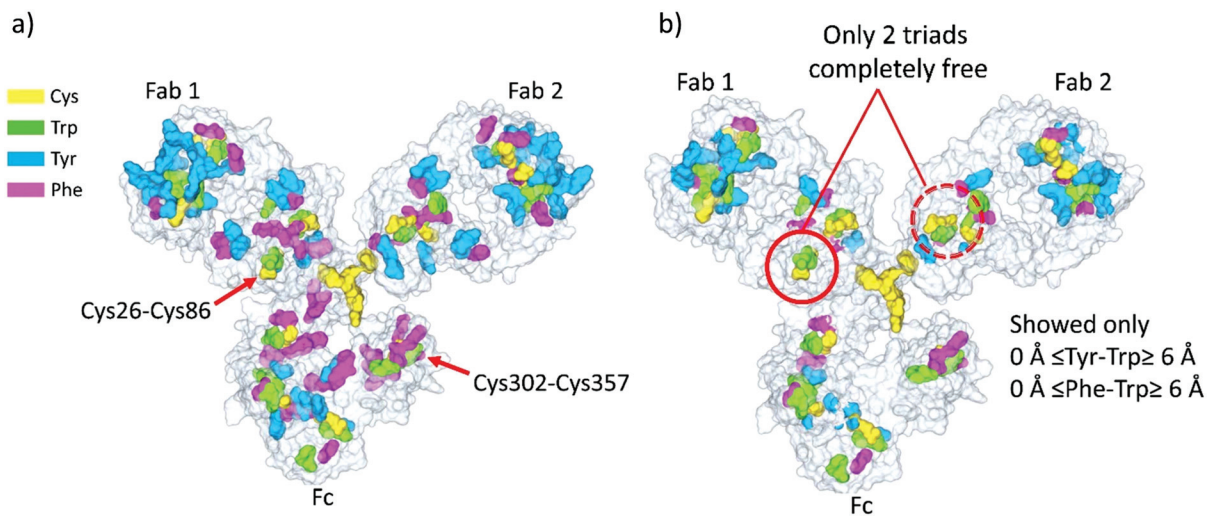

Fig. 5 3D structure of IgG 1IgY taken from the Protein Data Bank (PDB) showing (a) all the aromatic amino acids and cysteines. In (b) the same picture is reported with aromatic amino acids whose distance from the triad is smaller than 6 Å.

the selectivity of the UV irradiation under PIT conditions can be ascribed either to a shielding role played by tyrosine and phenylalanine, which hampers the bridge reduction, or to a poor exposition to the solvent as it is the case for C302–C357. We conclude that UV-treated antibodies can anchor a surface only through reduced cysteines C26 and C86.

Concerning the geometry established by the Ab, once immobilized on a surface, further insights come from evaluating flexibility and dynamics shown by these proteins in solution. As suggested by AFM and SAXS investigation,[65,66] the distribution of the angle ϑ between the two Fab domains (Fig. 6a) is quite peaked around 120°. On the opposite, the distribution of the angle between the normals to the domain planes is almost uniform in the range 10° to 90°. These results demonstrate the high flexibility of the Ab conformation also revealing that the flat-on position (Fig. 2) is quite unlikely.[65] Since our analysis suggests the immobilization by the thiol produced in the variable part of the light chain, we can conclude that the side-on position is more likely when PIT is applied as displayed in Fig. 6b. In fact, by considering the high flexibility of the Abs, we deduce that, even if one Fab domain is bound to the surface, all the possible orientations within the range $10° < \varphi < 90°$ can be experienced by the other Fab domain. These conclusions are consistent with a previous hypothesis about the Ab orientation induced by PIT.[42] Moreover, they highlight the convenience of using such a functionalization strategy since it leads at the same time to a strong (covalent) anchoring of Ab to the surface while orienting it side-on with one Fab exposed to the solution (Fig. 6b).

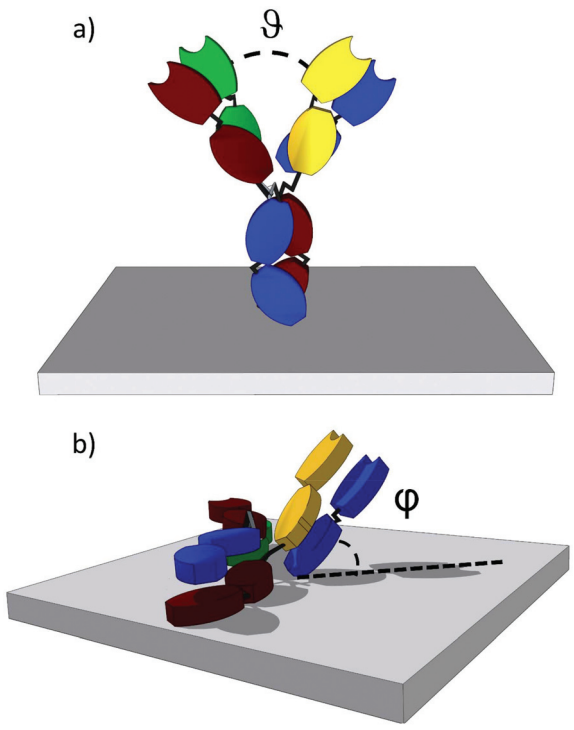

Fig. 6 (a) The angle ϑ between the two Fabs has a distribution peaked at approximately 120°. (b) IgG onto the surface in the position expected when PIT is realized. The angle φ spans almost uniformly the range 10° to 90° thereby providing one Fab well-exposed to the solvent.

4. Conclusions

Our work has demonstrated the effectiveness of PIT in the selective breaking of the disulfide bridges in IgG antibody, thereby producing highly reactive free thiols. These steer Ab to a convenient orientation of the Fab region once immobilized onto a metal surface. As an immediate consequence, this technique offers a powerful tool to significantly increase the number of effective antigen binding sites available onto any metal transducer. The presented photochemical functionalization method opens interesting perspectives in the sensor research since a wide range of highly sensitive and specific biosensing technologies employing Abs as biorecognition elements (*e.g.* antibody microarray devices)[67] would take advantage of it, thus greatly enhancing their performances. PIT is brilliantly competitive against alternative methods to anchor proteins onto metal surfaces, since it prevents the use of expensive toxic chemical reagents that require long and complex chemical procedures in well-equipped laboratories. In contrast, PIT can be safely run by non-expert personnel; it is rapid and user-friendly.

Measurements carried out by Ellman's assay, MS and SERS allowed us to identify the reduced cysteines produced by PIT and to unequivocally highlight the process behind PIT. Moreover, knowing the exact location of the reactive disulphide bridges, it was possible to simulate the position and the different geometries that IgGs can assume on planar surfaces after covalent PIT-induced anchoring.

Conflicts of interest

There are no conflicts to declare.

Acknowledgements

P. M., M. de A. and M. B. acknowledge financial support from the Tuscany Region in the framework of the POR-FESR 2014–2020 program Action 1.1.5.a3.

References

1 G. Rong, S. R. Corrie and H. A. Clark, *ACS Sens.*, 2017, **2**, 327–338.
2 Z. Farka, T. Juřík, D. Kovář, L. Trnková and P. Skládal, *Chem. Rev.*, 2017, **117**, 9973–10042.
3 S. M. Borisov and O. S. Wolfbeis, *Chem. Rev.*, 2008, **108**, 423–461.
4 D. Grieshaber, R. MacKenzie, J. Vörös and E. Reimhult, *Sensors*, 2008, **8**, 1400–1458.

5 A. K. Trilling, J. Beekwilder and H. Zuilhof, *Analyst*, 2013, **138**, 1619–1627.
6 A. Makaraviciute and A. Ramanaviciene, *Biosens. Bioelectron.*, 2013, **50**, 460–471.
7 Y. Du and S. Dong, *Anal. Chem.*, 2017, **89**, 189–215.
8 N. Aliakbarinodehi, P. Jolly, N. Bhalla, A. Miodek, G. De Micheli, P. Estrela and S. Carrara, *Sci. Rep.*, 2017, **7**, 44409.
9 A. Poma, A. P. F. Turner and S. A. Piletsky, *Trends Biotechnol.*, 2010, **28**, 629–637.
10 L. Uzun and A. P. F. Turner, *Biosens. Bioelectron.*, 2016, **76**, 131–144.
11 K. Mosbach and O. Ramström, *Nat. Biotechnol.*, 1996, **14**, 163–170.
12 E. V. Piletska, A. R. Guerreiro, M. J. Whitcombe and S. A. Piletsky, *Macromolecules*, 2009, **42**, 4921–4928.
13 S. K. Vashist and J. H. T. Luong, in *Handbook of Immunoassay Technologies*, Elsevier, Weinheim, Germany, 2018, vol. 3–4, pp. 1–18.
14 P. J. Conroy, S. Hearty, P. Leonard and R. J. O'Kennedy, *Semin. Cell Dev. Biol.*, 2009, **20**, 10–26.
15 S. Sharma, H. Byrne and R. J. O'Kennedy, *Essays Biochem.*, 2016, **60**, 9–18.
16 A. K. Trilling, M. M. Harmsen, V. J. B. Ruigrok, H. Zuilhof and J. Beekwilder, *Biosens. Bioelectron.*, 2013, **40**, 219–226.
17 M. Shen, J. F. Rusling and C. K. Dixit, *Methods*, 2017, **116**, 95–111.
18 L. S. Wong, F. Khan and J. Micklefield, *Chem. Rev.*, 2009, **109**, 4025–4053.
19 N. G. Welch, J. A. Scoble, B. W. Muir and P. J. Pigram, *Biointerphases*, 2017, **12**, 02D301.
20 Y. Jung, J. Y. Jeong and B. H. Chung, *Analyst*, 2008, **133**, 697–701.
21 S. K. Vashist, C. K. Dixit, B. D. MacCraith and R. O'Kennedy, *Analyst*, 2011, **136**, 4431–4436.
22 Y. Lee, J. Jeong, G. Lee, J. H. Moon and M. K. Lee, *Anal. Chem.*, 2016, **88**, 9503–9509.
23 M. T. Neves-Petersen, O. S. Gonçalves, M.-J. Bañuls, R. Alonso, P. Jiménez-Meneses, Á. Maquieira, H. Vorum and S. B. Petersen, in *Biophotonics: Photonic Solutions for Better Health Care VI*, ed. J. Popp, V. V. Tuchin and F. S. Pavone, SPIE, 2018, p. 106.
24 H. Sharma and R. Mutharasan, *Anal. Chem.*, 2013, **85**, 2472–2477.
25 S. Wu, H. Liu, X. M. Liang, X. Wu, B. Wang and Q. Zhang, *Anal. Chem.*, 2014, **86**, 4271–4277.
26 M. Pal, S. Lee, D. Kwon, J. Hwang, H. Lee, S. Hwang and S. Jeon, *Anal. Chim. Acta*, 2017, **952**, 81–87.
27 R. Alonso, P. Jiménez-Meneses, J. García-Rupérez, M. J. Bañuls and Á. Maquieira, *Chem. Commun.*, 2018, **54**, 6144–6147.
28 M. T. Neves-Petersen, G. P. Gajula and S. B. Petersen, in *Molecular Photochemistry - Various Aspects*, ed. S. Saha, InTech, Rijeka, 2012, pp. 125–158.
29 M. T. Neves-Petersen, T. Snabe, S. Klitgaard, M. E. G. Duroux and S. B. Petersen, *Protein Sci.*, 2006, **15**, 343–351.
30 A. Parracino, G. P. Gajula, A. K. di Gennaro, M. Correia, M. T. Neves-Petersen, J. Rafaelsen and S. B. Petersen, *Biotechnol. Bioeng.*, 2011, **108**, 999–1010.
31 A. Makaraviciute, C. D. Jackson, P. A. Millner and A. Ramanaviciene, *J. Immunol. Methods*, 2016, **429**, 50–56.
32 M. Iijima and S. Kuroda, *Biosens. Bioelectron.*, 2017, **89**, 810–821.
33 M. T. Neves-Petersen, Z. Gryczynski, J. Lakowicz, P. Fojan, S. Pedersen, E. Petersen and S. Bjørn Petersen, *Protein Sci.*, 2002, **11**, 588–600.
34 T. R. Ioerger, C. Du and D. S. Linthicum, *Mol. Immunol.*, 1999, **36**, 373–386.
35 R. Funari, B. Della Ventura, L. Schiavo, R. Esposito, C. Altucci and R. Velotta, *Anal. Chem.*, 2013, **85**, 6392–6397.
36 R. Funari, B. Della Ventura, R. Carrieri, L. Morra, E. Lahoz, F. Gesuele, C. Altucci and R. Velotta, *Biosens. Bioelectron.*, 2015, **67**, 224–229.
37 B. Della Ventura, N. Sakač, R. Funari and R. Velotta, *Talanta*, 2017, **174**, 52–58.
38 B. Della Ventura, L. Schiavo, C. Altucci, R. Esposito and R. Velotta, *Biomed. Opt. Express*, 2011, **2**, 3223–3231.
39 A. Fulgione, M. Cimafonte, B. Della Ventura, M. Iannaccone, C. Ambrosino, F. Capuano, Y. T. R. Proroga, R. Velotta and R. Capparelli, *Sci. Rep.*, 2018, **8**, 16137.
40 M. Iarossi, C. Schiattarella, I. Rea, L. De Stefano, R. Fittipaldi, A. Vecchione, R. Velotta and B. Della Ventura, *ACS Omega*, 2018, **3**, 3805–3812.
41 B. Della Ventura, M. Gelzo, E. Battista, A. Alabastri, A. Schirato, G. Castaldo, G. Corso, F. Gentile and R. Velotta, *ACS Appl. Mater. Interfaces*, 2019, **11**, 3753–3762.
42 R. Funari, B. Della Ventura, C. Altucci, A. Offenhäusser, D. Mayer and R. Velotta, *Langmuir*, 2016, **32**, 8084–8091.
43 L. J. Harris, E. Skaletsky and A. McPherson, *J. Mol. Biol.*, 1998, **275**, 861–872.
44 M. T. Neves-Petersen, S. Klitgaard, T. Pascher, E. Skovsen, T. Polivka, A. Yartsev, V. Sundström and S. B. Petersen, *Biophys. J.*, 2009, **97**, 211–226.
45 F. Reincke, S. G. Hickey, W. K. Kegel and D. Vanmaekelbergh, *Angew. Chem., Int. Ed.*, 2004, **43**, 458–462.
46 P. Matteini, M. De Angelis, L. Ulivi, S. Centi and R. Pini, *Nanoscale*, 2015, **7**, 3474–3480.
47 G. Sauerbrey, *Z. Phys.*, 1959, **155**, 206–222.
48 G. L. Ellman, *Arch. Biochem. Biophys.*, 1959, **82**, 70–77.
49 L. Dai, R. Preston, M. Bacica, A. Kinhikar, B. Bolaños and R. E. Murphy, *Bioconjugate Chem.*, 2013, **24**, 53–62.
50 W. Pusch and M. Kostrzewa, *Curr. Pharm. Des.*, 2005, **11**, 2577–2591.
51 A. Amoresano, A. Carpentieri, C. Giangrande, A. Palmese, G. Chiappetta, G. Marino and P. Pucci, *Clin. Chem. Lab. Med.*, 2009, **47**, 647–665.
52 Y. Yefremova, M. Al-Majdoub, K. F. M. Opuni, C. Koy, W. Cui, Y. Yan, M. L. Gross and M. O. Glocker, *J. Am. Soc. Mass Spectrom.*, 2015, **26**, 482–492.
53 N. M. Gevondyan, A. M. Volynskaia and V. S. Gevondyan, *Biochemistry*, 2006, **71**, 279–284.

54 L. M. Amzel and R. J. Poljak, *Annu. Rev. Biochem.*, 1979, **48**, 961–997.
55 H. Kikuchi, Y. Goto and K. Hamaguchi, *Biochemistry*, 1986, **25**, 2009–2013.
56 M. Banchelli, B. Tiribilli, M. de Angelis, R. Pini, G. Caminati and P. Matteini, *ACS Appl. Mater. Interfaces*, 2016, **8**, 2628–2634.
57 M. Rycenga, X. Xia, C. H. Moran, F. Zhou, D. Qin, Z. Y. Li and Y. Xia, *Angew. Chem., Int. Ed.*, 2011, **50**, 5473–5477.
58 J. Feng, J. M. Slocik, M. Sarikaya, R. R. Naik, B. L. Farmer and H. Heinz, *Small*, 2012, **8**, 1049–1059.
59 F. Tavanti, A. Pedone, P. Matteini and M. C. Menziani, *J. Phys. Chem. B*, 2017, **121**, 9532–9540.
60 L. Guo, J. A. Jackman, H. H. Yang, P. Chen, N. J. Cho and D. H. Kim, *Nano Today*, 2015, **10**, 213–239.
61 P. Matteini, M. Cottat, F. Tavanti, E. Panfilova, M. Scuderi, G. Nicotra, M. C. Menziani, N. Khlebtsov, M. De Angelis and R. Pini, *ACS Nano*, 2017, **11**, 918–926.
62 I. Martina, R. Wiesinger and M. Schreiner, *e-Preserv. Sci.*, 2012, **9**, 1–8.
63 E. Podstawka, Y. Ozaki and L. M. Proniewicz, *Appl. Spectrosc.*, 2004, **58**, 1147–1156.
64 G. Tomasello, Protein Imager 2.0. Retrieved from https://3dproteinimaging.com/.
65 X. Zhang, L. Zhang, H. Tong, B. Peng, M. J. Rames, S. Zhang and G. Ren, *Sci. Rep.*, 2015, **5**, 9803.
66 Q. Chen, M. Vieth, D. E. Timm, C. Humblet, D. Schneidman-Duhovny, I. E. Chemmama, A. Sali, W. Zeng, J. Lu and L. Liu, *PLoS One*, 2017, **12**, e0175758.
67 D. B. Bush and T. A. Knotts, *J. Chem. Phys.*, 2018, **149**, 165102.